MOLECULAR IMAGING AND BIOLOGY

Mol Imaging Biol (2019) 21:731–739
DOI: 10.1007/s11307-018-1295-7

Published Online: 19 November 2018

RESEARCH ARTICLE

Apparent Diffusion Coefficient Histogram Analysis for Assessing Tumor Staging and Detection of Lymph Node Metastasis in Epithelial Ovarian Cancer: Correlation with p53 and Ki-67 Expression

Feng Wang,[1] Yuxiang Wang,[2] Yan Zhou,[1] Congrong Liu,[2] Dong Liang,[3] Lizhi Xie,[4] Zhihang Yao,[1] Jianyu Liu[1]

[1]*Department of Radiology, Peking University Third Hospital, 49 North Garden Street, Haidian District, Beijing, 100191, China*
[2]*Department of Pathology, School of Basic Medical Science, Peking University Third Hospital, Peking University Health Science Center, 38 Xueyuan Road, Haidian District, Beijing, 100191, China*
[3]*Siemens Ltd., China, 7 Wangjing Zhonghuan Nanlu, Chaoyang District, Beijing, 100102, China*
[4]*GE Healthcare China, 1 Yongchang North Road, Beijing, 100176, China*

Abstract

Purpose: To investigate the potential of apparent diffusion coefficient (ADC) histogram parameters in epithelial ovarian cancer (EOC) for distinguishing different tumor stages and determining lymph node status and correlations between ADC values and p53 and Ki-67 expression.

Procedures: Forty-nine EOC patients underwent preoperative magnetic resonance imaging. Staging and lymph node status were determined postoperatively. ADC values were measured using histogram analysis and compared between groups. Relationships between ADCs and Ki-67 and p53 expression were explored.

Results: DC parameters differed significantly between stage I *vs* II, I *vs* III, and I *vs* IV. The parameters were significantly lower in the lymph node-positive group than in the lymph node-negative group, were significantly negatively correlated with Ki-67 labeling index, and were all significantly lower in the mutation-type p53 group than in the wild-type p53 group.

Conclusions: ADC histogram analysis can help discriminate stage I from advanced-stage EOC and predict lymph node metastasis. ADC parameters were correlated with Ki-67 labeling index; the parameters may help indicate p53 expression.

Key words: Lymph nodes, Magnetic resonance imaging, Neoplasm metastasis, Neoplasm staging, Ovarian cancer

Introduction

Epithelial ovarian cancer (EOC) is the second most common gynecologic malignancy and the leading cause of gynecologic cancer deaths [1]. Accurate staging is important for the selection of an appropriate treatment strategy and prognostic

Feng Wang and Yuxiang Wang should be considered co-first authors.

Correspondence to: Jianyu Liu; *e-mail:* jyliubysy@163.com

evaluation [2]. Lymph node status directly affects the determination of the International Federation of Gynecology and Obstetrics (FIGO) stage of EOC. Although exploratory laparotomy and histological examination of the specimens obtained are currently the gold standard methods for staging in all women suspected of having EOC, it is necessary to explore less invasive preoperative methods for the evaluation of tumor stage and lymph node metastasis [3]. Furthermore, patients with stage I disease and those suitable for neoadjuvant chemotherapy would benefit from accurate preoperative assessment [4–6].

Recent studies indicate that the combination of magnetic resonance imaging (MRI) and diffusion-weighted imaging (DWI) may be a promising tool for staging tumors, but its performance in the detection of lymph node metastasis is evidently less than satisfactory [7]. Historically, the assessment of lymph node status has depended mainly on morphological features, and some small lymph node metastases have been undetectable [3, 6, 7]. Therefore, it is necessary to explore the histological characteristics of metastatic lymph nodes. Moreover, in order to avoid situations where it is difficult to place the region of interest (ROI) on small lymph nodes, new detection methods need to be developed. Lymph node metastasis has been shown to be linked to histological characteristics and imaging findings of the primary tumor in a variety of conditions, including gastric cancer, cervical cancer, and pancreatic neuroendocrine tumor [8–10]. For example, in some previous reports, poorly differentiated tumors were more likely to be associated with lymph node metastasis [11, 12]. Thus, exploration of the primary tumor in cases of EOC may yield valuable information about tumor dissemination.

DWI utilizes the Brownian motion of water molecules to reveal the microstructural features of tissue such as cellularity and microcirculation [13, 14]. The apparent diffusion coefficient (ADC) is a quantitative parameter calculated *via* DWI. Restricted diffusion of water molecules results in high signal intensity on DWI and a low ADC value, while free diffusion results in low signal intensity and a high ADC value. ADC mapping has been applied in cases of EOC to assist in the differential diagnosis of benign and malignant lesions, determination of tumor grade, and assessment of treatment responses [14]. Notably however, most previous studies have measured ADC values by placing a localized ROI on several representative sections of the tumor. Such a method can result in sampling bias and interobserver variability with regard to ROI selection [15].

A histogram analysis approach that involves encompassing the whole tumor has shown great promise for the characterization of tumor tissue. ADC values of all voxels within the tumor contribute to the histogram, and tissue components with different diffusion features can be reflected in the histogram, giving rise to the objectivity, repeatability, and comprehensiveness of this approach [9, 15, 16].

The aims of the current study were to investigate correlations between ADC histogram parameters and tumor stages, particularly lymph node status, and correlations between ADC values and p53 and Ki-67 expression—which are important diagnostic markers for EOC.

Materials and Methods

Patients

The current study was approved by the relevant institutional review board, it was conducted in accordance with the ethical standards laid down in the 1964 Declaration of Helsinki and its later amendments, and written informed consent was obtained from all individual participants included in the study. A total of 49 patients (mean age 53.4 ± 10.4 years) who underwent preoperative MRI examination including DWI and subsequently had diagnoses of EOC confirmed *via* postoperative pathology were enrolled in the study. None of the patients had received radiotherapy, chemotherapy, or any other treatment prior to MRI examination. Patients in which the maximum diameter of the primary lesion was < 1.0 cm (n = 2) were excluded, because it was difficult to calculate DWI histogram parameters for lesions of this size.

MRI Technique

All MRI examinations were performed using a 3.0-T system (Discovery MR750, GE Healthcare, USA) with an eight-channel cardiac array coil. Patients fasted for 4–6 h, then hyoscine butylbromide (20 mg) was injected intramuscularly prior to image acquisition to reduce bowel peristalsis artifacts. Conventional imaging protocols were as follows: axial T1-weighted fast spin-echo (FSE) imaging with repetition time (TR)/echo time (TE) of 452–850/7 ms, slice thickness/intersection gap of 5.0 mm/1.0 mm, bandwidth of 62.5 kHz, field of view of 32 cm × 32 cm, matrix of 320 × 224, and axial, sagittal, and coronal T2-weighted fast recovery FSE images (TR/TE 4453–7830/98–106 ms, slice thickness/intersection gap 4.0 mm/0.4 mm, bandwidth 62.5 kHz, field of view 22 cm × 22 cm, matrix 288 × 288). Dynamic contrast-enhanced (DCE) MRI was performed before and immediately after the intravenous injection of gadolinium diethylenetriaminepentaacetic acid (Gd-DTPA) contrast agent (0.2 mmol/kg at a rate of 2 ml/s) with T1-weighted liver acquisition of volume acceleration in the axial plane (TR/TE 3.05/1.44 ms, slice thickness/intersection gap 4.0 mm/−2 mm, bandwidth 125 kHz, field of view 34 cm × 34 cm, matrix 288 × 192).

Before the injection of Gd-DTPA, axial DWI was performed using free-breathing single-shot echo-planar

Table 1.. Histopathological diagnosis of patients

Groups	*N* (%)
Subtype	
High-grade serous carcinomas	33 (67.3)
Clear cell carcinomas	7 (14.3)
Endometrioid carcinomas	6 (12.2)
Low-grade serous carcinomas	1 (2.0)
Brenner tumor	1 (2.0)
Seromucinous carcinoma	1 (2.0)
Laterality	
Unilateral	35 (71.4)
Bilateral	14 (28.6)
FIGO stage	
I	10 (20.4)
II	8 (16.3)
III	25 (51.0)
IV	6 (12.2)
Lymph node metastasis	
N–	29 (59.2)
N+	20 (40.8)
p53 expression	
mu-p53	32 (65.3)
wt-p53	17 (34.7)

imaging sequences acquired using the following parameters: TR/TE 2600/71.5 ms, slice thickness/intersection gap 5.0 mm/1.0 mm, bandwidth 250 kHz, field of view 34 cm × 34 cm, matrix 160 × 160, and parallel imaging factor 2. Eleven *b* values (0 s/mm^2, 30 s/mm^2, 50 s/mm^2, 100 s/mm^2, 150 s/mm^2, 200 s/mm^2, 400 s/mm^2, 600 s/mm^2, 800 s/mm^2, 1000 s/mm^2, 1500 s/mm^2) were used, and the acquisition time was 2 min and 44 s.

Image Analysis

Two abdominal radiologists, one with 8 years of gynecologic imaging experience and the other with 3 years of gynecologic imaging experience, reviewed the DWI and MRI data *via* a workstation (AW 4.5, GE) without any knowledge of the surgical, pathologic, or other imaging staging information. Using conventional and DCE MRI scans as references, ROIs were manually drawn on all continuous DWI slices (b = 1000 s/mm^2) that encompassed all the solid components of the ovarian lesions, for both unilateral and bilateral lesions. Necrotic, cystic, and hemorrhagic areas of tumors and artifacts were excluded to the greatest extent possible. Quantitative ADC maps were generated automatically *via* built-in software (Functool MADC, GE). The obtained volumes of interest (VOIs) of whole tumors and ADC maps were then converted in DICOM format and imported into MATLAB software, in order to copy the VOIs from the DWI images to the same locations in the ADC maps. The means, medians, and 10th and 90th percentiles of ADC values were then computed *via* histogram analysis.

Histopathologic Analysis

In all cases, diagnoses, staging, and lymph node status were confirmed by postoperative histopathology. The FIGO staging system was used to determine EOC stages,

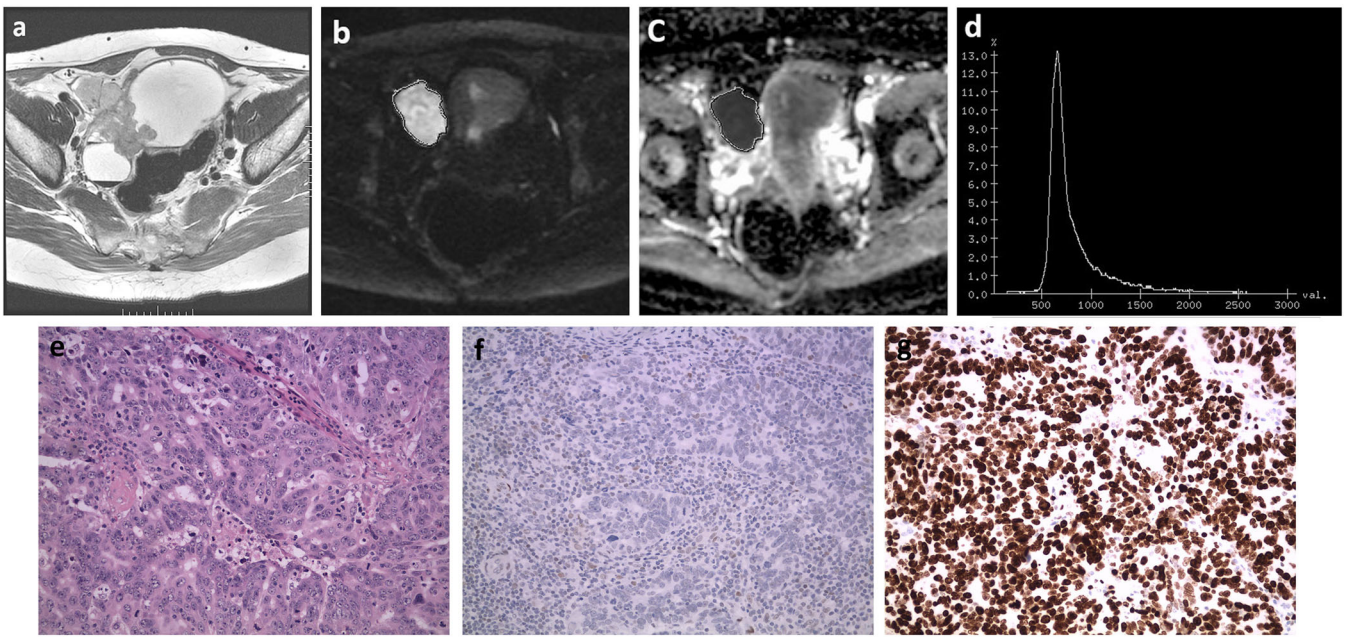

Fig. 1. A 45-year-old woman with stage IIIA1 EOC. **a** Axial T2-weighted MRI revealed a solid and cystic mass on the right adnexa. **b** The solid components of the tumor were hyperintense in DWI (b = 1000 s/mm^2), but **c** hypointense in ADC mapping. **d** An ADC histogram was generated. **e** Photomicrography (hematoxylin-eosin staining, × 200) revealed high-grade serous carcinoma. **f** p53 staining depicted a complete absence of expression (mu-p53). **g** The Ki-67 LI was 95 %.

Table 2.. ADC histogram parameters for discriminating different groups of epithelial ovarian cancer

Parameter	Stage					Lymph node metastasis		
	I	II	III	IV	*p*	N−	N+	*p*
ADC_{mean}	1.43 ± 0.22	1.16 ± 0.19	1.07 ± 0.17	1.05 ± 0.19	*0.000*	1.25 ± 0.22	1.01 ± 0.17	*0.000*
ADC_{10th}	1.05 ± 0.20	0.84 ± 0.13	0.78 ± 0.13	0.77 ± 0.16	*0.000*	0.91 ± 0.18	0.75 ± 0.14	*0.002*
ADC_{90th}	1.94 ± 0.28	1.60 ± 0.28	1.48 ± 0.22	1.43 ± 0.32	*0.000*	1.73 ± 0.28	1.38 ± 0.22	*0.000*
ADC_{median}	1.35 ± 0.22	1.10 ± 0.20	1.00 ± 0.19	0.90 ± 0.23	*0.000*	1.16 ± 0.25	0.94 ± 0.17	*0.001*

ADC histogram parameters are presented as means ± standard deviations. Data are given as $\times 10^{-3}$ mm^2/s. Significant differences are captured in italics

which were grouped into stages I to IV. Based on whether there was lymph node metastasis or not, cases were divided into lymph node-positive (N+) and lymph node-negative (N−) groups. Immunohistochemistry investigations of p53 and Ki-67 were conducted, and the results were analyzed by a pathologist with more than 10 years of relevant experience. Deparaffinization, rehydration, antigen retrieval, and serum blocking were followed by incubation with primary antibody at 37 °C for 1 h. The primary antibodies included p53 (clone DO-7, DAKO, Glostrup, Denmark) and Ki-67 (clone MIB-1, DAKO). Incubation with the secondary antibody was conducted for 30 min at room temperature, followed by DAB staining. Ki-67 labeling index (LI) was defined as the percentage of positive cells. Expression of p53 was categorized as wild-type (wt-p53) or mutation-type (mu-p53), based on whether expression was focal or diffuse and strongly nuclear or completely absent, respectively.

Statistical Analysis

MedCalc 11.4 and SPSS 23.0 statistical software packages were used for statistical analysis. The normality of ADC and Ki-67 LI data sets was evaluated using the Kolmogorov-Smirnov test. Differences in ADC parameters at different stages were assessed *via* one-way analysis of variance (ANOVA), and subsequent comparisons between pairs of groups were analyzed *via* the post hoc least significant difference *t*-test. The *t*-test for independent groups was used to evaluate differences in ADC parameters between N+ and N− groups and between the two p53 staining patterns. Receiver operating characteristic (ROC) curves were generated to assess the diagnostic capacities of the ADC histogram parameters for the identification of specific tumor stages and lymph node status. The areas under the ROC curves (AUCs) of ADC parameters were then compared with each other to analyze differences in performance. Correlations between Ki-67 LI and ADC parameters were assessed *via* Pearson's correlation analysis. A p value < 0.05 was deemed to indicate statistical significance.

Results

Clinical and Histopathological Findings

Histopathological patient diagnoses are presented in Table 1. In brief, there were 10 stage I EOCs (mean patient age 51.1 ± 9.9 years), 8 stage II EOCs (55.4 ± 12.8 years), 25 stage III EOCs (53.4 ± 9.7 years), and 6 stage IV EOCs (54.8 ± 13.1 years). Lymph node metastases were detected in 20 cases (mean patient age 52.1 ± 10.8 years), while the other 29 cases (mean patient age 55.3 ± 9.9 years) were lymph node-negative. Fig. 1 shows a representative case.

Comparison of ADC Histogram Parameters Between Different Groups

The mean, median, and 10th and 90th ADC percentiles of EOCs at all four different stages differed significantly ($p < 0.05$) (Table 2). Notably, all histogram parameters decreased as tumor staging increased. In pairwise comparisons, ADC parameters were significantly lower in stage I than in stages II, III, and IV ($p < 0.05$) (Table 3). However, there were no significant differences

Table 3.. Pairwise comparison of the ADC histogram parameters for different stages of epithelial ovarian cancer

Parameter	Stage I *vs* II	Stage I *vs* III	Stage I *vs* IV	Stage II *vs* III	Stage II *vs* IV	Stage III *vs* IV
ADC_{mean}	*0.004*	*0.000*	*0.000*	0.248	0.258	0.754
ADC_{10th}	*0.005*	*0.000*	*0.001*	0.333	0.398	0.889
ADC_{90th}	*0.006*	*0.000*	*0.000*	0.249	0.232	0.694
ADC_{median}	*0.011*	*0.000*	*0.000*	0.221	0.074	0.294

Significant differences are captured in italics

Table 4.. Results of ROC analysis for the ADC histogram parameters

Parameter	AUC	Cutoff value*	Accuracy	Sensitivity	Specificity	PPV	NPV	*p* value
Stage I *vs* II + III + IV								
ADC_{mean}	0.895	1.254	0.857 (42/49)	0.900 (9/10)	0.846 (33/39)	0.600 (9/15)	0.971 (33/34)	0.000
ADC_{10th}	0.892	0.900	0.796 (39/49)	0.900 (9/10)	0.769 (30/39)	0.500 (9/18)	0.968 (30/31)	0.000
ADC_{90th}	0.886	1.883	0.898 (44/49)	0.700 (7/10)	0.949 (37/39)	0.778 (7/9)	0.925 (37/40)	0.000
ADC_{median}	0.888	1.160	0.837 (41/49)	0.900 (9/10)	0.821 (32/39)	0.563 (9/16)	0.970 (32/33)	0.000
N+ *vs* N−								
ADC_{mean}	0.815	1.003	0.796 (39/49)	0.600 (12/20)	0.931 (27/29)	0.857 (12/14)	0.771 (27/35)	0.000
ADC_{10th}	0.767	0.787	0.755 (37/49)	0.650 (13/20)	0.828 (24/29)	0.722 (13/18)	0.774 (24/31)	0.002
ADC_{90th}	0.825	1.639	0.714 (35/49)	0.900 (18/20)	0.586 (17/29)	0.600 (18/30)	0.895 (17/19)	0.000
ADC_{median}	0.772	0.934	0.755 (37/49)	0.600 (12/20)	0.862 (25/29)	0.750 (12/16)	0.758 (25/33)	0.001

PPV positive predictive value, *NPV* negative predictive value
*Units of $\times 10^{-3}$ mm^2/s for the ADC histogram parameters

in ADC parameters between any two of the three advanced stages (*i.e.*, stages II, III, and IV). The ADC histogram parameters in the N+ group were significantly lower than those in the N− group ($p < 0.05$).

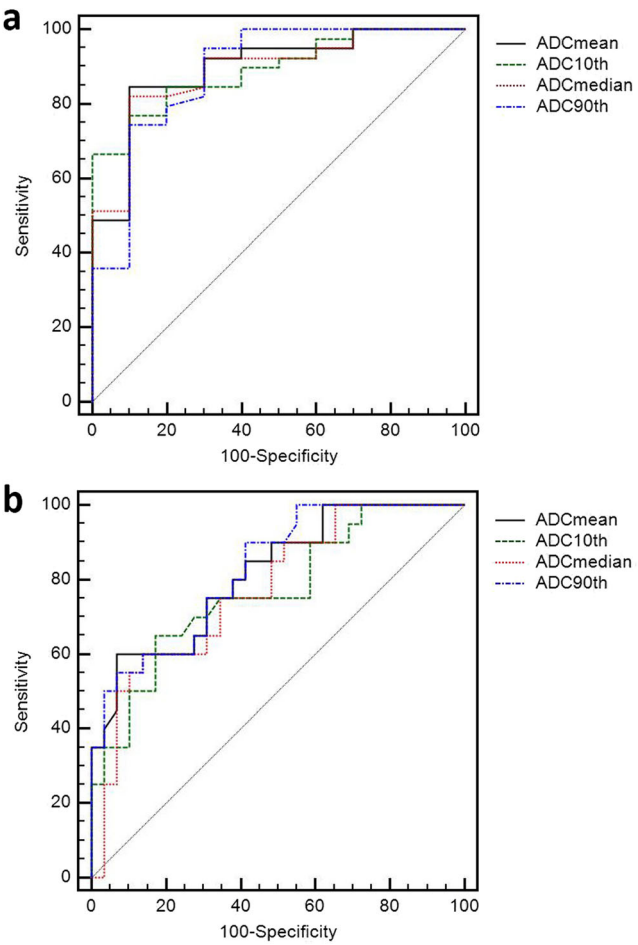

Fig. 2. ROC analysis of the ADC histogram parameters. **a** ROC curves of the ADC histogram parameters for the identification of stage I tumors. **b** ROC curves of ADC parameters for the identification of EOCs with lymph node metastasis. There were no significant differences between any two ROC curves ($p > 0.05$).

Diagnostic Performance of ADC Histogram Parameters

In the ROC analysis, all of the ADC histogram parameters (mean, median, 10th and 90th percentile) performed well with regard to the identification of stage I tumors and N+ status (Table 4, Fig. 2). ADC means were associated with the highest AUC for the detection of stage I tumors, while the 90th ADC percentile was associated with the highest AUC for differentiating between N− and N+—but none of these differences were statistically significant.

Relationships Between ADC Histogram Parameters and p53 and Ki-67 Expression

ADC parameters were all significantly lower in the mu-p53 group than in the wt-p53 group (mean 1.06 ± 0.16 *vs* 1.33 ± 0.23 × 10^{-3} mm^2/s, 10th percentile 0.77 ± 0.13 *vs* 0.98 ± 0.20 × 10^{-3} mm^2/s, 90th percentile 1.47 ± 0.24 *vs* 1.81 ± 0.31 × 10^{-3} mm^2/s, and median 0.97 ± 0.19 *vs* 1.26 ± 0.24 × 10^{-3} mm^2/s; all $p < 0.001$; Fig. 3), and there were significant negative correlations between ADC parameters and Ki-67 LI values (Fig. 4).

Discussion

The present study demonstrated the potential of an ADC histogram analysis approach to differentiate between tumor stages and determine lymph node status in cases of EOC. Previous reports have suggested that quantitative ADC analysis may be useful for evaluating the subtype, grade, and stage of ovarian cancers and predicting responses to chemotherapy [17–20]. The present study supports such findings pertaining to tumor staging, which have rarely been reported, and it is the first reported study exploring relationships between ADC values and lymphatic metastasis in cases of EOC. Moreover, in the current study, the ADC histogram parameters were associated with p53 and Ki-67 expression in EOCs.

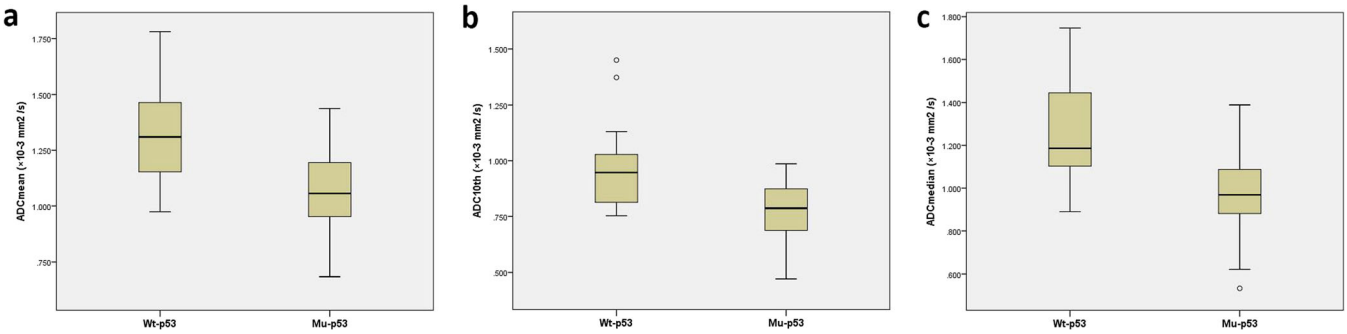

Fig. 3. **a–c** Relationship between the ADC histogram parameters and p53 expression. ADC values in the wt-p53 group were significantly higher than those in the mu-p53 group.

Morphological analysis *via* traditional imaging technologies is currently utilized for the preoperative staging of EOCs, but notably, ADC histogram analysis provides additional information that is correlated with EOC aggressiveness. In the current study, early-stage (stage I) EOCs exhibited higher ADCs than advanced-stage (II–IV) EOCs, which is consistent with the results reported by Oh *et al.* [18]. As the tumor progresses, changes in the tumor microenvironment enhance the proliferative ability of the tumor cells and increase their metastatic capacity [21–23]. ADC values based on water molecular diffusion may reflect the microstructure of relevant tissues in this respect. Therefore, compared with early-stage EOCs, increased cellular density in advanced-stage tumors may result in decreased ADC values. We surmise that there may be two other reasons for the aforementioned differences. One pertains to the fact that some studies have indicated that advanced- and early-stage ovarian cancers may develop *via* separate molecular pathways and may have different metastatic potentials [24, 25]. Another consideration is that

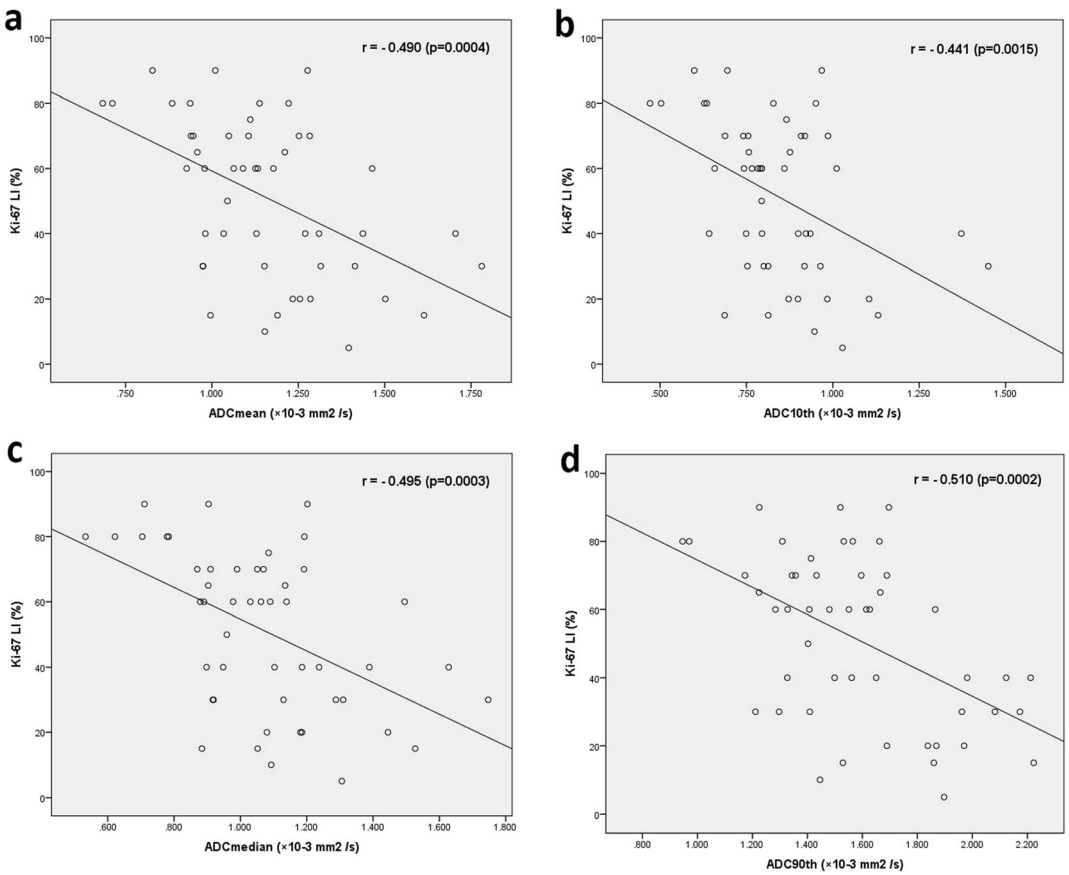

Fig. 4. **a–d** ADC histogram parameters and Ki-67 LI were significantly negatively correlated.

the epithelial-mesenchymal transition (EMT), through which ovarian cancer cells acquire an invasive capacity, may be associated with tumor ADC values [9, 22, 26]. These two considerations may also be relevant to the fact that in the current study, there were no significant differences between the ADCs of any two of the three advanced tumor stages. Fortunately, the identification of stage I tumor limited to one or both adnexa may be useful for the selection of an appropriate treatment method, especially in patients who wish to maintain fertility [5].

Unsurprisingly, compared with the N− group, ADC values were reduced in the N+ group, indicating higher cellular density of the primary tumor. Lymph node metastasis is associated with various factors, of which certain characteristics of the primary tumor play pivotal roles [11, 27, 28]. Tumors with strong proliferative and metastatic capabilities may be associated with increased risks of lymphatic invasion [11, 28]. Notably, EMT has also recently been reported to be associated with lymphatic dissemination of cancer cells [9, 29]. Investigation of specific factors that contribute to lymphatic metastasis was beyond the scope of the present study, but in-depth explorations in this regard are planned in the future. While systematic lymphadenectomy is a routine treatment for EOC, the method is considered relatively invasive and high-risk [3, 30]. We suggest that the results of the current study may be valuable in the context of clarifying the mechanisms of lymphatic metastasis and developing novel methods for the diagnosis and treatment of EOCs associated with lymphatic metastasis.

Recently, several studies have analyzed the associations between ADC values and histopathological features like p53 and Ki-67 in different tumors and showed varying results [9, 31–38]. Some studies showed that ADC values correlated significantly with p53 expression in thyroid cancer [33], bladder cancer [32], and cervical cancer [9], whereas no significant correlation was found in liver metastases from colorectal cancers [31]. In our study, there were significant differences in the ADC histogram parameters between wt-p53 and mu-p53. Our results are different from some of the reported data in other tumors. This could be because of the fact that different tumors have different histologic features; another main reason could be the new p53 immunohistochemistry pattern of EOC that we used in this study, which was different from previous interpretation based on the percentage of stained tumor cell nuclei [39, 40]. p53 immunohistochemistry is a reliable alternative to the identification of TP53 mutational status [40–42]. Abnormal/mutation-type p53 is an almost certain indicator of an underlying TP53 mutation [40]. TP53 mutation is associated with tumorigenesis and a high rate of cellular proliferation in ovarian cancer [41, 42], which may lead to a decline in ADC values in mu-p53. Conversely, normal wt-p53 indicates the absence of TP53 mutation and is reportedly associated with relatively indolent tumor biology [40]. Unsurprisingly, there was a significant negative correlation between Ki-67 expression and ADC parameters in the current study. Although some studies did not find a significant correlation between ADC and Ki-67 [9, 36], our results are as expected and consistent with most reported data [31–34, 37, 38]. Further, the results are concordant with those reported by Lindgren et al. [43]. Ki-67 is an indicator of tumor proliferation [43–45]. Higher Ki-67 LI values correspond with higher proliferative activity of tumor cells and thus give rise to increased cellularity, which leads to the restricted diffusion of water molecules and a decrease in ADC values. The relationship between ADC values and immunohistochemical indexes in the present study suggests that ADC alteration may assist in the evaluation of tumor proliferation and the prediction of p53 expression in ovarian cancer.

EOC is heterogeneous, even within the same tumor [46]. Histogram-based VOI analysis can capture all voxels within the lesion and enables certain components to be selected and evaluated. All of the ADC histogram parameters performed well with regard to the identification of stage I tumors or EOCs with lymph node metastasis in the current study. Somewhat unexpectedly, ADC mean and ADC 90th percentiles were associated with the highest AUCs, although these observations were not statistically significant. In most previous studies, lower ADC percentile values have not performed better than higher ADC percentiles with respect to the differentiation of malignant tumors, because lower ADC percentiles were presumed to represent areas of higher cellularity, which may be the best indicator of relevant tumor features in this regard [47, 48]. Although the reason for this discrepancy in the current study remains unclear, we speculate that EOCs with tumor metastasis may have more microscopic necrosis, hemorrhage, and cysts, which contribute to higher ADC values [49], because in some studies, tumor necrosis factor has been linked to tumor invasion and metastasis [50, 51]. Further studies are certainly warranted in this respect.

The current study had several limitations. The relatively small study sample, particularly with regard to stage I EOCs, limits the applicability of the results. Additionally, we did not explore relationships between ADC values and histological markers of the aforementioned EMT in EOCs. Lastly, the study included several different histological EOC subtypes, which may be a potentially confounding factor. We plan to conduct a more comprehensive analysis in the future, in order to generate more informative results.

Conclusions

ADC histogram analysis can assist in the discrimination of stage I EOC from advanced-stage EOC and in the detection of lymph node metastasis. Moreover, ADC parameters were strongly correlated with Ki-67 LI and may help in indicating molecular changes such as p53 expression.

FundingThis study has received funding from the Capital Characteristic Clinic Project of China (Z131107002213049) and the Beijing Municipal Natural Science Foundation (7162102).

Compliance with Ethical Standards

Ethical Approval

All procedures performed in studies involving human participants were conducted in accordance with the ethical standards of the institutional and/or national research committee and with the 1964 Helsinki Declaration and its later amendments or comparable ethical standards.

Conflict of Interest

The authors declare that they have no conflict of interest.

References

1. Ramalingam P (2016) Morphologic, immunophenotypic, and molecular features of epithelial ovarian cancer. Oncology (Williston Park) 30:166–176
2. Booth SJ, Turnbull LW, Poole DR, Richmond I (2008) The accurate staging of ovarian cancer using 3T magnetic resonance imaging—a realistic option. BJOG 115:894–901
3. Pu T, Xiong L, Liu Q, Zhang M, Cai Q, Liu H, Sood AK, Li G, Kang Y, Xu C (2017) Delineation of retroperitoneal metastatic lymph nodes in ovarian cancer with near-infrared fluorescence imaging. Oncol Lett 14:2869–2877
4. Gomez-Hidalgo NR, Martinez-Cannon BA, Nick AM et al (2015) Predictors of optimal cytoreduction in patients with newly diagnosed advanced-stage epithelial ovarian cancer: time to incorporate laparoscopic assessment into the standard of care. Gynecol Oncol 137:553–558
5. Satoh T, Hatae M, Watanabe Y, Yaegashi N, Ishiko O, Kodama S, Yamaguchi S, Ochiai K, Takano M, Yokota H, Kawakami Y, Nishimura S, Ogishima D, Nakagawa S, Kobayashi H, Shiozawa T, Nakanishi T, Kamura T, Konishi I, Yoshikawa H (2010) Outcomes of fertility-sparing surgery for stage I epithelial ovarian cancer: a proposal for patient selection. J Clin Oncol 28:1727–1732
6. Yuan Y, Gu ZX, Tao XF, Liu SY (2012) Computer tomography, magnetic resonance imaging, and positron emission tomography or positron emission tomography/computer tomography for detection of metastatic lymph nodes in patients with ovarian cancer: a meta-analysis. Eur J Radiol 81:1002–1006
7. Michielsen K, Vergote I, Op de Beeck K et al (2014) Whole-body MRI with diffusion-weighted sequence for staging of patients with suspected ovarian cancer: a clinical feasibility study in comparison to CT and FDG-PET/CT. Eur Radiol 24:889–901
8. Liu S, Zhang Y, Chen L, Guan W, Guan Y, Ge Y, He J, Zhou Z (2017) Whole-lesion apparent diffusion coefficient histogram analysis: significance in T and N staging of gastric cancers. BMC Cancer 17:665
9. Schob S, Meyer HJ, Pazaitis N, Schramm D, Bremicker K, Exner M, Höhn AK, Garnov N, Surov A (2017) ADC histogram analysis of cervical cancer aids detecting lymphatic metastases—a preliminary study. Mol Imaging Biol 19:953–962
10. De Robertis R, Maris B, Cardobi N et al (2018) Can histogram analysis of MR images predict aggressiveness in pancreatic neuroendocrine tumors? Eur Radiol 28:2582–2591. https://doi.org/10.1007/s00330-017-5236-7
11. Ayhan A, Gultekin M, Taskiran C, Celik NY, Usubutun A, Kucukali T, Yuce K (2005) Lymphatic metastasis in epithelial ovarian carcinoma with respect to clinicopathological variables. Gynecol Oncol 97:400–404
12. Xu YY, Huang BJ, Sun Z, Lu C, Liu YP (2007) Risk factors for lymph node metastasis and evaluation of reasonable surgery for early gastric cancer. World J Gastroenterol 13:5133–5138
13. Barral M, Taouli B, Guiu B, Koh DM, Luciani A, Manfredi R, Vilgrain V, Hoeffel C, Kanematsu M, Soyer P (2015) Diffusion-weighted MR imaging of the pancreas: current status and recommendations. Radiology 274:45–63
14. Rockall AG (2014) Diffusion weighted MRI in ovarian cancer. Curr Opin Oncol 26:529–535
15. Kang Y, Choi SH, Kim YJ, Kim KG, Sohn CH, Kim JH, Yun TJ, Chang KH (2011) Gliomas: histogram analysis of apparent diffusion coefficient maps with standard- or high-b-value diffusion-weighted MR imaging—correlation with tumor grade. Radiology 261:882–890
16. Zhang YD, Wang Q, Wu CJ, Wang XN, Zhang J, Liu H, Liu XS, Shi HB (2015) The histogram analysis of diffusion-weighted intravoxel incoherent motion (IVIM) imaging for differentiating the Gleason grade of prostate cancer. Eur Radiol 25:994–1004
17. Li HM, Qiang JW, Xia GL, Zhao SH, Ma FH, Cai SQ, Feng F, Fu AY (2015) MRI for differentiating ovarian endometrioid adenocarcinoma from high-grade serous adenocarcinoma. J Ovarian Res 8:26
18. Oh JW, Rha SE, Oh SN, Park MY, Byun JY, Lee A (2015) Diffusion-weighted MRI of epithelial ovarian cancers: correlation of apparent diffusion coefficient values with histologic grade and surgical stage. Eur J Radiol 84:590–595
19. Wang F, Wang Y, Zhou Y, Liu C, Xie L, Zhou Z, Liang D, Shen Y, Yao Z, Liu J (2017) Comparison between types I and II epithelial ovarian cancer using histogram analysis of monoexponential, biexponential, and stretched-exponential diffusion models. J Magn Reson Imaging 46:1797–1809
20. Kyriazi S, Collins DJ, Messiou C, Pennert K, Davidson RL, Giles SL, Kaye SB, deSouza NM (2011) Metastatic ovarian and primary peritoneal cancer: assessing chemotherapy response with diffusion-weighted MR imaging—value of histogram analysis of apparent diffusion coefficients. Radiology 261:182–192
21. Woo S, Lee JM, Yoon JH, Joo I et al (2014) Intravoxel incoherent motion diffusion-weighted MR imaging of hepatocellular carcinoma: correlation with enhancement degree and histologic grade. Radiology 270:758–767
22. Nakayama K, Nakayama N, Katagiri H, Miyazaki K (2012) Mechanisms of ovarian cancer metastasis: biochemical pathways. Int J Mol Sci 13:11705–11717
23. van Baal J, van Noorden CJF, Nieuwland R et al (2018) Development of peritoneal carcinomatosis in epithelial ovarian cancer: a review. J Histochem Cytochem 66:67–83
24. Zaal A, Peyrot WJ, Berns PM et al (2012) Genomic aberrations relate early and advanced stage ovarian cancer. Cell Oncol (Dordr) 35:181–188
25. Shridhar V, Lee J, Pandita A, Iturria S, Avula R, Staub J, Morrissey M, Calhoun E, Sen A, Kalli K, Keeney G, Roche P, Cliby W, Lu K, Schmandt R, Mills GB, Bast RC Jr, James CD, Couch FJ, Hartmann LC, Lillie J, Smith DI (2001) Genetic analysis of early- versus late-stage ovarian tumors. Cancer Res 61:5895–5904
26. Chen YW, Pan HB, Tseng HH, Chu HC, Hung YT, Yen YC, Chou CP (2013) Differentiated epithelial- and mesenchymal-like phenotypes in subcutaneous mouse xenografts using diffusion weighted-magnetic resonance imaging. Int J Mol Sci 14:21943–21959
27. Bogani G, Tagliabue E, Ditto A, Signorelli M, Martinelli F, Casarin J, Chiappa V, Dondi G, Leone Roberti Maggiore U, Scaffa C, Borghi C, Montanelli L, Lorusso D, Raspagliesi F (2017) Assessing the risk of pelvic and para-aortic nodal involvement in apparent early-stage ovarian cancer: a predictors- and nomogram-based analyses. Gynecol Oncol 147:61–65
28. Powless CA, Aletti GD, Bakkum-Gamez JN, Cliby WA (2011) Risk factors for lymph node metastasis in apparent early-stage epithelial ovarian cancer: implications for surgical staging. Gynecol Oncol 122:536–540
29. Karlsson MC, Gonzalez SF, Welin J, Fuxe J (2017) Epithelial-mesenchymal transition in cancer metastasis through the lymphatic system. Mol Oncol 11:781–791
30. Fan L, Liu Y, Zhang X, Kang Y, Xu C (2014) Establishment of Fischer 344 rat model of ovarian cancer with lymphatic metastasis. Arch Gynecol Obstet 289:149–154
31. Heijmen L, Ter Voert EE, Nagtegaal ID et al (2013) Diffusion-weighted MR imaging in liver metastases of colorectal cancer: reproducibility and biological validation. Eur Radiol 23:748–756
32. Sevcenco S, Haitel A, Ponhold L, Susani M, Fajkovic H, Shariat SF, Hiess M, Spick C, Szarvas T, Baltzer PAT (2014) Quantitative apparent diffusion coefficient measurements obtained by 3-tesla MRI are correlated with biomarkers of bladder cancer proliferative activity. PLoS One 9:e106866
33. Schob S, Meyer HJ, Dieckow J et al (2017) Histogram analysis of diffusion weighted imaging at 3T is useful for prediction of lymphatic metastatic spread, proliferative activity, and cellularity in thyroid cancer. Int J Mol Sci 18

34. Meyer HJ, Hohn A, Surov A (2018) Histogram analysis of ADC in rectal cancer: associations with different histopathological findings including expression of EGFR, Hif1-alpha, VEGF, p53, PD1, and KI 67. A preliminary study. Oncotarget 9:18510–18517
35. Meyer HJ, Leifels L, Hamerla G, Höhn AK, Surov A (2018) ADC-histogram analysis in head and neck squamous cell carcinoma. Associations with different histopathological features including expression of EGFR, VEGF, HIF-1alpha, Her 2 and p53. A preliminary study. Magn Reson Imaging 54:214–217
36. Meyer HJ, Pazaitis N, Surov A (2018) ADC histogram analysis of muscle lymphoma-correlation with histopathology in a rare entity. Br J Radiol 91:20180291
37. Shen L, Zhou G, Tong T, Tang F, Lin Y, Zhou J, Wang Y, Zong G, Zhang L (2018) ADC at 3.0T as a noninvasive biomarker for preoperative prediction of Ki67 expression in invasive ductal carcinoma of breast. Clin Imaging 52:16–22
38. Surov A, Meyer HJ, Winter K, Richter C, Hoehn AK (2018) Histogram analysis parameters of apparent diffusion coefficient reflect tumor cellularity and proliferation activity in head and neck squamous cell carcinoma. Oncotarget 9:23599–23607
39. Kobel M, Piskorz AM, Lee S et al (2016) Optimized p53 immunohistochemistry is an accurate predictor of TP53 mutation in ovarian carcinoma. J Pathol Clin Res 2:247–258
40. Casey L, Kobel M, Ganesan R et al (2017) A comparison of p53 and WT1 immunohistochemical expression patterns in tubo-ovarian high-grade serous carcinoma before and after neoadjuvant chemotherapy. Histopathology 71:736–742
41. Sallum LF, Andrade L, Ramalho S, Ferracini AC, de Andrade Natal R, Brito ABC, Sarian LO, Derchain S (2018) WT1, p53 and p16 expression in the diagnosis of low- and high-grade serous ovarian carcinomas and their relation to prognosis. Oncotarget 9:15818–15827
42. Kobel M, Ronnett BM, Singh N et al (2018) Interpretation of P53 immunohistochemistry in endometrial carcinomas: toward increased reproducibility. Int J Gynecol Pathol. https://doi.org/10.1097/PGP.0000000000000488
43. Lindgren A, Anttila M, Rautiainen S, Arponen O, Kivelä A, Mäkinen P, Härmä K, Hämäläinen K, Kosma VM, Ylä-Herttuala S, Vanninen R, Sallinen H (2017) Primary and metastatic ovarian cancer: characterization by 3.0T diffusion-weighted MRI. Eur Radiol 27:4002–4012
44. Surov A, Meyer HJ, Wienke A (2017) Associations between apparent diffusion coefficient (ADC) and KI 67 in different tumors: a meta-analysis. Part 1: ADCmean. Oncotarget 8:75434–75444
45. Li HM, Zhao SH, Qiang JW, Zhang GF, Feng F, Ma FH, Li YA, Gu WY (2017) Diffusion kurtosis imaging for differentiating borderline from malignant epithelial ovarian tumors: a correlation with Ki-67 expression. J Magn Reson Imaging 46:1499–1506
46. Bilyk O, Coatham M, Jewer M, Postovit LM (2017) Epithelial-to-mesenchymal transition in the female reproductive tract: from normal functioning to disease pathology. Front Oncol 7:145
47. Hao Y, Pan C, Chen W, Li T, Zhu WZ, Qi JP (2016) Differentiation between malignant and benign thyroid nodules and stratification of papillary thyroid cancer with aggressive histological features: whole-lesion diffusion-weighted imaging histogram analysis. J Magn Reson Imaging 44:1546–1555. https://doi.org/10.1002/jmri.25290
48. Suo S, Zhang K, Cao M, Suo X, Hua J, Geng X, Chen J, Zhuang Z, Ji X, Lu Q, Wang H, Xu J (2016) Characterization of breast masses as benign or malignant at 3.0T MRI with whole-lesion histogram analysis of the apparent diffusion coefficient. J Magn Reson Imaging 43:894–902
49. Li X, Yuan Y, Ren J, Shi Y, Tao X (2018) Incremental prognostic value of apparent diffusion coefficient histogram analysis in head and neck squamous cell carcinoma. Acad Radiol 25:1433–1438. https://doi.org/10.1016/j.acra.2018.02.017
50. Maolake A, Izumi K, Natsagdorj A, Iwamoto H, Kadomoto S, Makino T, Naito R, Shigehara K, Kadono Y, Hiratsuka K, Wufuer G, Nastiuk KL, Mizokami A (2018) Tumor necrosis factor-alpha induces prostate cancer cell migration in lymphatic metastasis through CCR7 upregulation. Cancer Sci 109:1524–1531. https://doi.org/10.1111/cas.13586
51. Liang Y, Jiao J, Liang L, Zhang J, Lu Y, Xie H, Liang Q, Wan D, Duan L, Wu Y, Zhang B (2018) Tumor necrosis factor receptor-associated factor 6 mediated the promotion of salivary adenoid cystic carcinoma progression through Smad-p38-JNK signaling pathway induced by TGF-beta. J Oral Pathol Med 47:583–589. https://doi.org/10.1111/jop.12709